Indian J. Phys. 79(6), 623-630 (2005)

AN INTERNATIONAL JOURNAL
IJP

Gaseous clusters as targets for use in laser plasma interaction experiments

S Sailaja*, R A Khan, S R Kumbhare, P A Naik and P D Gupta

Laser Plasma Division, Centre for Advanced Technology, Indore-452 013, Madhya Pradesh, India

E-mail : ssailaja@indiatimes.com

Received 30 July 2004, accepted 16 March 2005

Abstract : We have carried out various characterisation studies for different sonic and hypersonic nozzles, to optimise cluster formation in gas jets. Studies were done to decide optimum laser focus position for the nozzles and also to determine the best nozzle for laser-cluster interaction experiments. Argon gas cluster targets were irradiated by 1.5 J/25 ps laser pulses, from the fundamental beam of our Nd : phosphate glass laser. X-ray pinhole imaging of the laser produced cluster plasmas revealed information about the plasma column in the gas jet. High laser energy absorption of 80–85% was observed for argon clusters, and this was consistent with the intense X-ray emission signals measured using filtered X-ray PIN diodes.

Keywords : Laser produced plasma, clusters, gas puff targets.

PACS Nos. : 36.40.Gk, 52.50.Jm

1. Introduction

The high intensity pulsed X-ray emission from laser produced plasmas has drawn considerable attention of researchers due to its wide ranging applications in many fields such as indirect drive in inertial confinement fusion [1], XUV – soft X-ray lasers [2], X-ray contact microscopy of live biological cells in the water window region [3], soft X-ray microlithography [4] *etc*. In the latter two applications, the use of solid targets has a definite disadvantage due to severe debris problem, which causes damage to the specimen. Several novel techniques like the use of cryogenically cooled liquid droplet targets [5], tape targets [6], and the use of background gas [6] have been explored by researchers in this field to reduce the contamination due to debris. The operation of droplet sources requires cryogenic cooling and is relatively difficult to achieve, whereas the latter two methods only reduce the debris and do not eliminate it. Pulsed gas jet targets offer an attractive alternative and are currently used in a wide range of physics experiments [7–14], particularly in laser-plasma interaction studies with intense short pulse lasers [7–10]. Such gas jets are essentially debris-free sources, due to the target being a gas at room temperature and also have the advantage of high repetition rate of operation. The irradiation of gas puffs results in production of uniform hot plasma free of severe density gradients, which is ideal for X-ray lasing applications [2]. However, irradiation of gas puff targets results in low X-ray yield, as the laser light is weakly absorbed in gases due to lower densities as compared to solids [14]. However, experiments conducted over the last few years by several groups [7–10] have shown that the interaction of short duration (< 1 ps), intense (10^{16}–10^{18} W cm^{-2}) laser pulses with clusters (10^2–10^7 atoms/cluster) produced in gas jets can result in near total absorption of laser light. A detailed review on the subject of laser-cluster interactions is given in Ref. [12]. Such clusters form an intermediate state between atoms or small molecules and solids, having the same local density as a solid, but an overall average gas density. They can be considered as small spherical balls of nanometer dimension, whose radius is much smaller than the laser wavelength. Thus,

*Corresponding Author
Corresponding Address : 1/1 Ground Floor, Royal Garden, 12, Park Avenue, K. P. Puram, Chennai-600 028, India

© 2005 IACS

the laser light can be absorbed very efficiently in these near solid density clusters, as their size is usually of the order of the skin depth (~100 Å) of the laser. The efficient heating of the cluster due to collisional processes and the complex cluster dynamics of resonant absorption, lead to high X-ray conversions. The heated cluster explodes due to thermal and Coulomb pressure ejecting very hot electrons and ions. For example, irradiation of cryogenically cooled D_2 clusters leads to very fast deuterium ions, which are ejected from the exploding cluster. Fusion reaction events of the type ${}_1D^2 + {}_1D^2 \rightarrow {}_2He^3 + {}_0n^1$ can then occur with high probability leading to emission of 2.45 MeV neutrons. Fusion yields of 10^5 neutrons per joule of laser energy have been reported [15].

Most experiments involving clusters have been carried out using ultra-short (<1 ps), intense (10^{16}–10^{18} W cm^{-2}) laser pulses. The existing theoretical models for femtosecond to sub-picosecond laser-cluster interaction predict that clusters would explode on the sub-picosecond timescale and therefore, a high degree of laser absorption and intense X-ray emission would be possible only for ultra-short laser pulses. However, we have observed that the irradiation of clusters with moderately intense lasers of tens of picosecond duration can still result in efficient absorption of laser energy and may lead to X-ray emission comparable to that of solid targets under similar parameters.

A detailed study of the various nozzle parameters and optimisation of the operating conditions is necessary, for maximising the X-ray yield. In this paper, we report on the characterisation of various nozzles used, the confirmation of cluster formation through Rayleigh scattering techniques and the spatial profile measurements of cluster distribution in the gas jet. In all our experiments, we have used argon gas to form clusters. We have also carried out initial measurements of X-ray emission from argon cluster plasmas, produced from laser irradiation of these cluster targets with a 1.5 J/25 ps Nd : Phosphate glass laser, using filtered X-ray PIN diodes. 2-D X-ray imaging studies of the cluster plasma were done using an X-ray pinhole camera.

2. Cluster size estimation

Gas jets or puffs are generated by the pulsed injection of a small amount of gas at high pressure into a vacuum chamber by means of a solenoid valve. The gas undergoes adiabatic cooling as it expands at the expense of its internal energy, and its random thermal energy is converted to directed kinetic energy. The gas supersaturates and nucleates under the influence of van der Waal's forces forming clusters of solid density. The size and nature of these clusters are determined by the nozzle geometry, condensation parameter, backing pressure and stagnation temperature of the gas used [16,17].

There is no rigorous theory for predicting the onset of cluster formation. The clustering is determined by a semi-empirical formula called the Hagena scaling parameter [16]. Figures 1 (a, b) show the typical sonic

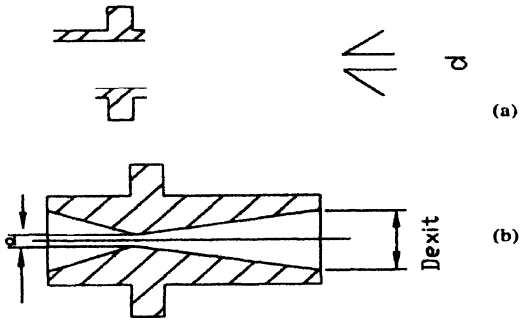

Figure 1. Diagram of a typical (a) sonic nozzle, (b) hypersonic nozzle.

and hypersonic nozzles used in our experiments. The scaling parameter Γ^*, is given by the expression.

$$\Gamma^* = k[d\ (\mu m)/\tan\ \alpha]^{0.85}\ p_0\ (\text{mbar})/T^{2.29}, \quad (1)$$

$$N_C = 33\ [\Gamma^*/1000]^{1.95-2.35}, \quad (2)$$

where N_C is the average cluster size in number of atoms per cluster, k, p_0, and T are the condensation parameter, stagnation pressure and temperature of the gas respectively, d is the throat diameter and α is the half cone angle of the nozzle. For the three nozzles used in our experiments, these parameters were : (a) hypersonic nozzle : d = 1 mm ϕ (jet throat diameter), D_{exit} = 3 mm ϕ, α = 5°; (b) hypersonic nozzle : d = 0.5 mm ϕ (jet throat diameter), D_{exit} = 2.5 mm ϕ, and α = 5°; and (c) sonic nozzle : d = 1.3 mm ϕ, α = 45°.

The formation of clusters in a gas puff and an approximate estimation of its size can be made by using Rayleigh scattering techniques. The experimental set up is given in Figure 2. Light from a 2 mW green He-Ne laser (λ = 0.543 μm) used as a probe beam was incident on the gas jet, and the sideways scattered signal at 90° to the probe beam, was collected using an imaging lens of 5 cm ϕ and 5 cm focal length. It was imaged with a magnification of 2X onto a pinhole of 2 mm ϕ, which was part of the light tight housing placed in front of the photo multiplier tube (PMT) detector, to avoid spurious signals. The experiments were carried out in 10^{-3} torr.

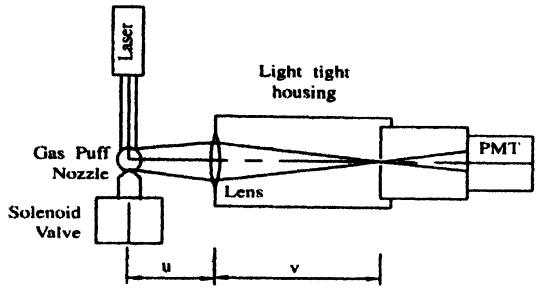

Figure 2. Experimental set-up for Rayleigh scattering measurements.

With the onset of cluster formation, the radius of the scattering element increases and hence also the Rayleigh scattered signal. In fact, the Rayleigh scattered signal S_{RS} is expected to have a near cubic dependence on backing pressure, when clustering takes place [7]. The variation of Rayleigh scattered signal (S_{RS}) with backing pressure (p_0) for various nozzles is shown in Figure 3. Our observation of the dependence of the signal on the backing pressure ($S_{RS} \propto p_0^{\beta}$), where β varied from 2.5 – 4.0, for the different nozzles, confirmed the presence of clusters in the gas jet.

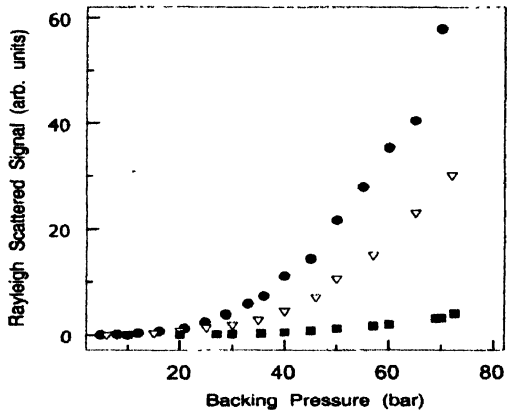

Figure 3. Variation of Rayleigh scattered signal with backing pressure for ● — hypersonic nozzle (d = 1 mm, D_{exit} = 3 mm, α = 5°); ▽ — hypersonic nozzle (d = 0.5 mm, D_{exit} = 2.5 mm, α = 5°); ■ — sonic nozzle (d = 1.3 mm, α = 45°).

3. Characteristion of gas jets/cluster jets at the nozzle output

For laser plasma experiments, it would be desirable to focus the laser beam at the position where the gas jet has maximum density. This would occur just at the exit of the nozzle. However, in order to avoid degradation to the nozzle either directly by the laser or by the ions produced in the plasma [5,13], it is required to focus the laser beyond a certain minimum distance from the nozzle exit. A distance of 2–3 mm was found to be optimum. In all our laser plasma experiments described in this paper, involving irradiation of gas puff targets, the laser was focussed at a height of ~2 mm from the nozzle.

3.1. Spatial profile of cluster distribution along the radial direction :

It is desirable to align the gas jet in the laser focus position, such that the highest laser intensity is achieved at a position where the cluster size and density are maximum. This is required to ensure maximum laser absorption at the desired laser intensity. Therefore, an imaging experiment was set up to find out the cluster spatial profile along the radial direction at a height of ~2 mm from the nozzle output. The experimental set up is similar to that shown in Figure 2, except that the nozzle is placed in the horizontal position and light from a 2 mW green He-Ne laser (λ = 0.543 μm) was made incident on it at 90° angle. The experiments were carried in an interaction chamber evacuated to ~10^{-4} torr. A convex lens viewing the nozzle along its axial direction imaged the Rayleigh scattered signal on to a (ICCD) camera with 2X magnification. A light tight housing was provided to reduce the background noise level.

This geometric configuration has the advantage that it does not require either deconvolution of the laser intensity profile or Abel inversion of the intensity profile of the scattered signal. The horizontal scan of the image at the central position gives the spatial profile of the convolution of the cluster density (number of clusters/ unit volume) and the cluster size along the radial direction. Figure 4 shows the typical spatial profiles of the Rayleigh scattered signal for different nozzles. It should be noted that

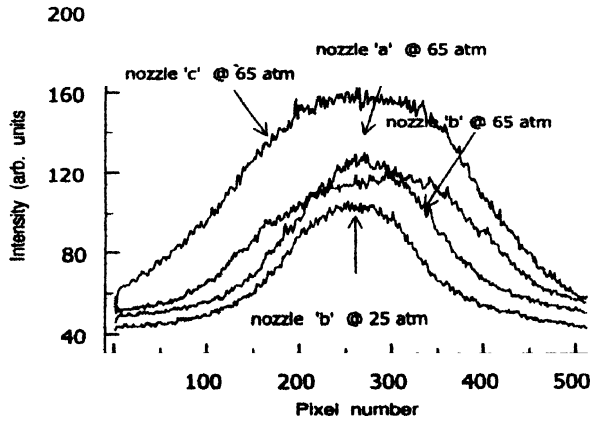

Figure 4. Typical spatial profiles of Rayleigh scattered for different nozzles : (a) hypersonic nozzle (d = 1 mm, D_{exit} = 3 mm, α = 5°); (b) hypersonic nozzle (d = 0.5 mm, D_{exit} = 2.5 mm, α = 5°); (c) sonic nozzle (d = 1.3 mm, α = 45°).

different filters were used for recording signals from different nozzles and the relative peak intensities are therefore, not representative of the true signal strengths.

3.2. Interferometric measurement of average gas density in the vicinity of the nozzle output :

Figure 5 shows a schematic of the experimental set up for density estimation using a Jamin interferometer configuration. The nozzle was placed in the path of an

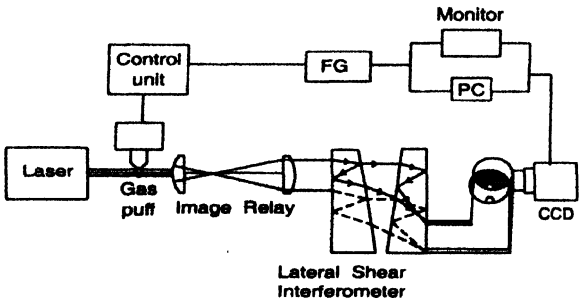

Figure 5. Schematic diagram of the experimental set-up for density estimation using Jamin interferometer configuration.

expanded He-Ne laser beam (λ = 0.6328 μm). An image relay system was used to image the nozzle output onto a CCD camera detector with 2X magnification, through the Jamin interferometer. This lens system also collimates the He-Ne beam and provides a further 2X beam expansion. The lateral shear introduced by the Jamin interferometer produced fringes of ~175 μm width on the camera. Argon gas was puffed through the hypersonic nozzle (d = 1 mm ϕ, D_{exit} = 3 mm ϕ, α = 5°) and sonic nozzle (d = 1.3 mm ϕ, α = 45°) at different backing pressures. The refractive index η of the argon gas jet was derived from the measured fringe shift. The average gas density N at the nozzle output was then estimated using the relation, $N = (\eta^2 - 1)\, N_m/3A$, where N_m is Avagadro number and A is the molar refractivity of argon [18]. The gas density at the nozzle output, is higher in a sonic nozzle due to its geometry, as compared to the hypersonic case. However, since clustering depends on adiabatic cooling as well, which is more in hypersonic or conical geometry, clusters of larger size are formed at the same or even lower backing pressures in gas jets emanating from hypersonic nozzles.

4. X-ray pinhole imaging of laser produced gas plasma

X-ray pinhole imaging of laser produced argon gas plasma was carried out using an on-line X-ray pinhole camera, as shown in Figure 6. The object distance and image

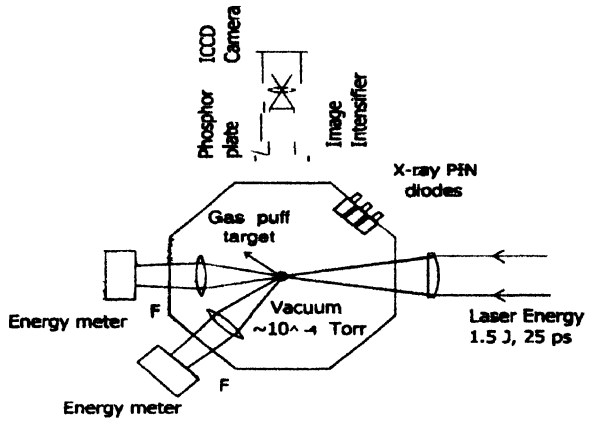

Figure 6. Schematic diagram of experimental set-up for laser energy absorption measurements.

distance were u = 11 cm and v = 33 cm respectively, resulting in a magnification of 3X. The pinhole aperture was 50 μm ϕ, and 1 B-10 aluminised polycarbonate foil with $h\nu_{cutoff}$ = 0.8 keV, was used to block the visible light. A phosphor coated fiber optic plate (P-22 phosphor with Al coating) was placed at the detector end. X-rays incident on this phosphor are down converted to visible light and transmitted through the fiber optic plate. The visible image had a 1 : 1 correspondence with the X-ray pinhole image incident on the phosphor. This plate was coupled to an image intensifier tube through another fiber optic plate placed in physical contact with it. The output of the image intensifier tube was coupled to an ICCD camera through an imaging lens. The de-magnified image was read out by the ICCD camera and stored in digital form in the PC for further analysis.

Figures 7 (a, b, c) show the X-ray pinhole pictures of laser produced argon plasma at 30, 40, and 70 bar backing pressure respectively. Plasma was created by irradiating the argon gas target puffed out of the hypersonic nozzle (d = 1 mm ϕ, D_{exit} = 3 mm ϕ, and α = 5°), by light from our Nd : Phosphate glass laser (λ_L = 1.054 μm, E_L = 1.5 J/25 ps). The Gaussian focal spot was 35 μm radius, giving maximum laser irradiation of ~10^{15} W cm^{-2}. Laser breakdown in a gas is a function of both light intensity and gas density. As the Rayleigh range of our laser is ~3.5 mm, the focussed intensity can be considered to be approximately constant in the laser focal region at the nozzle output (when there is no gas puff present). The laser is aligned for best focus by monitoring the X-ray signals on the PIN diodes.

5. Laser energy absorption experiments

Figure 6 also shows a schematic diagram of the experimental set-up used to carry out measurements of

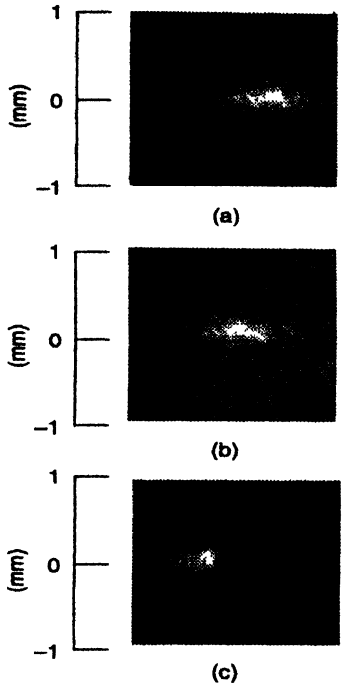

Figure 7. X-Ray pinhole pictures of laser produced argon plasma at (a) 30 bar, (b) 40 bar and (c) 70 bar.

laser energy absorption in the gas jet. The laser energy absorption was studied from measurements of the percentage of transmitted and scattered laser light [9,13]. An *f*/4 convex lens was used to collect the transmitted light on to an energy meter and the collection solid angle of the lens was kept large enough, to ensure that any refracted light from the plasma was collected onto the energy meter. Another *f*/2 convex lens kept at 45° to the laser beam axis, was used to collect the sideways-scattered light. RG 1000 IR pass filters were used to block all visible light from the plasma.

A Parker solenoid valve obtained from General Valve Corporation, was used to puff the gases in to the vacuum chamber. The hypersonic nozzle with d = 1 mm ϕ (jet throat diameter), D_{exit} = 3 mm ϕ, and α = 5° (half cone angle) was used in our experiments. Rayleigh scattering techniques were used to synchronize firing of the laser with the maximum cluster size reached during the opening of the valve.

Figure 8 shows the variation of laser absorption with incident laser intensity at different backing pressures. At p_0 = 15 bar, it is seen that absorption reaches a maximum at an intensity, I_L ~2 × 10^{14} W cm^{-2} and then decreases with increasing intensities. However, for p_0 = 40 bar and 60 bar, absorption increases steadily with intensity when I_L < 5 × 10^{14} W cm^{-2}, after which it remains constant, thereafter showing a decreasing trend for I_L > 10^{15} W cm^{-2}. We have observed maximum energy absorption of the order of ~80–85%. This high absorption is consistent with the intense X-ray signals observed through X-ray PIN diodes. Figure 9 shows the steady increase in X-ray signals (PIN diode with 2B-10 aluminised polycarbonate filter, $h\nu_{cutoff}$ = 1.1 keV) with increasing backing pressure, and hence cluster size. To the best of our knowledge, such high laser light absorption for low Z and medium Z gases has not been observed in earlier work reported by other groups, for such simple nozzle geometry, in the high energy, multi-picosecond regime [19].

6. Results and discussion

From the results of Rayleigh scattering experiments in Figure 3, it is seen that for the case of the hypersonic nozzle, the scattered signal is weaker for a jet throat diameter of d = 0.5 mm than for d = 1 mm. This is as expected as the cluster size is expected to decrease about four times for the same gas parameters (N_C α d^2). It is well established that the gas puff undergoes greater cooling when the aperture is larger. Besides, the gas density is also expected to be higher for larger diameters due to smaller impedance. Further, the scattered signal S_{RS} for the sonic nozzles and hence clustering is observed to be much smaller, than for the hypersonic nozzles with similar throat diameter d. The relation is given by d_{eq}/d = 0.74/tan α, where d_{eq} is the equivalent throat diameter for a sonic nozzle, d and α are the actual throat diameter and the half cone angle of the hypersonic nozzle [16,17]. It would therefore, be more desirable to use a hypersonic nozzle of an equivalent throat diameter, as for the same clustering, the gas throughput is reduced by (8.4^2 = 70), ~seventy times, thus reducing the load on vacuum requirements. Therefore, hypersonic nozzles are clearly superior to sonic nozzles for experiments involving cluster targets.

From measurements of spatial profile of cluster distribution along the radial direction, as shown in Figure 4, the half cone divergence angle of the gas jet was estimated to be ~7° for the hypersonic and ~27° for the sonic nozzle. In general, gas jets with a smaller spatial extent (FWHM), uniform radial profile and gas flow with low divergence are desirable, for efficient absorption of the laser beam. It is noted that these conditions are more easily satisfied using hypersonic nozzles.

The X-ray pinhole pictures in Figure 7 (a, b, c) shown that the laser breakdown occurs earlier for higher

backing pressures varying from 1.4 mm @ 30 bar, 1.7 mm @ 40 bar to 2.2 mm @ 70 bar, away from the geometric centre of the nozzle (towards the focussing lens). This is due to prior breakdown of laser because of higher gas densities present in the vicinity of the nozzle output at higher backing pressures. The peak of the X-ray emission is also seen to shift away from the nozzle centre in a similar manner, with increasing backing pressure. The peak X-ray emission region was noted to be at 0.65 mm @ 30 bar, 1.0 mm @ 40 bar and 1.5 mm @ 70 bar, away with respect to the geometric centre of the nozzle (towards the focussing lens). The width of the plasma column was found to be ~150 μm at all pressures, and its length varied from ~1.2 mm @ 30–40 bar to 0.9 mm @ 70 bar. The X-ray emission region was slightly smaller at higher pressures.

From a knowledge of the laser focal volume, coupled with energy absorption results and measurements of gas density at the nozzle output, one can calculate approximately the laser energy deposited per atom [9]. From interferometric measurements described in Section 3.2, the average gas density at nozzle output (hypersonic nozzle) was determined to be ~8 × 10^{19} atoms cm^{-3} for a backing pressure of 60 bar. The laser focal volume was calculated to be ~4 × 10^{-6} cm^3 (considering the plasma focal volume to be a cylinder, with a focal radius of 35 μm, and length of 1 mm). There are about ~3.2 × 10^{14} atoms in the focal volume. For an absorbed energy of ~1 J, approximately a maximum of 3 × 10^{-8} erg or 19 keV of energy is deposited per single atom. This is in broad agreement with the maximum ion energies ranging from ~8–25 keV indicated for high charge (>9) states, using time of flight measurement, reported earlier [11]. In practical situations, due to the Gaussian spatial profile of the laser beam, the intensity at the wings is much smaller than at the center. Besides, the energy and hence the intensity, decreases rapidly due to absorption as the laser traverses the length of the gas column. Therefore, the energy deposited per atom at different positions in the focal volume would be widely different.

Laser irradiation of gas puff targets typically results in low conversions. Besides, even for laser irradiation of gas cluster targets, efficient absorption of laser energy was not indicated from earlier work for long duration pulses (greater than several picoseconds). However, we have observed that the initial presence of clusters in the gas puff can create conditions for the efficient absorption of laser energy on long time scales (tens of picosecond) and the mechanisms of laser absorption are indicated as follows [19]. Initial ionisation is created in the clusters, due to multiphoton processes in the leading edge of the pulse. The electrons acquire quiver energy U_P (eV) ~9.33 × 10^{-14} I_L λ^2 W cm^{-2} μm^2, of ~10–45 eV as they oscillate in the electric field of the laser at irradiation intensities of I_L ~1–5 × 10^{14} W cm^{-2}. The cluster gets heated due to electron-ion collisions and begins to expand under hydrodynamic pressure. Resonance absorption takes place when the plasma density reaches three time the critical density [7] of the laser, leading to intense heating of the cluster and further ionisation to higher charge states. This process would take several picoseconds. The expansion of the solid density cluster due to thermal pressure brings it to bulk plasma density. The larger clusters not only take longer time to come to resonance, owing to slower hydrodynamic expansion, but also stay close to resonance for a longer duration. Due to the high atomic densities present in the interaction region, the plasma density after significant ionisation, would still be near critical, even after disassembling of the clusters. Thus, the continued efficient absorption of laser light in the sub-critical density plasma takes place through out the focal volume. This could explain both our results of highly efficient absorption and strong X-ray signals measured by the X-ray PIN diodes.

The variation of energy absorption with laser intensity is dependent on several factors. At backing pressures p_0 = 15, 40 and 60 bar, considering the two different scalings given by eq. (2), the average range of cluster sizes in terms of cluster radius are r_C ~170–330 Å, 320–720 Å and 425–990 Å, respectively. The typical plasma temperature expected from our irradiation conditions is of the order of 100 eV, which would give an expansion speed of c_s ~5 × 10^6 cm/sec. The hydrodynamic time scale taken to reach critical density, is given by τ_{crit} ~ $(n_e/n_{crit})^{1/3}$. r_C/c_s, [7] where n_e ~1.5 × 10^{23} cm^{-3} and n_{crit} are the initial electron density in the cluster and critical density respectively. For p_0 = 15, 40, and 60 bar, taking averaged values of cluster radius, these would be 2.8 ps, 5.8 ps and 8 ps, and the bulk plasma densities in the interaction region, after disassembling of the clusters, would be ~0.16 n_{crit}, 0.43 n_{crit} and 0.64 n_{crit}, respectively. (For a backing pressure of 60 bar, as the measured gas density in argon was estimated to be ~8 × 10^{19} atoms cm^{-3} and the average ionisation state in argon plasma was 8 [19], the electron density would be equal to the product *i.e.* 6.4 × 10^{20} cm^{-3}). At low intensities, especially

due to the Gaussian temporal and spatial profile of the laser beam, the ionisation thresholds are not reached in the leading edge of the pulse, and sufficient ionisation of all the clusters in the focal volume does not take place, leading to decreased absorption. However, at higher incident laser intensity, once the critical intensity for ionisation threshold is reached at an optimum time in the leading edge of the pulse, further increase in the laser intensity does not lead to increased absorption. This happens because it is offset by another mechanism, which is the cluster expansion [7]. If sufficient threshold intensity is reached too early in the pulse, as would happen at higher laser intensity, the cluster would expand too fast and come to resonance very early in the laser pulse. Thus, the efficient absorption of the laser energy in the near solid density cluster through inverse bremstrahlung and at resonance are reduced, thereby decreasing the laser energy absorption. Obviously, there is an optimum intensity for the most efficient absorption and it should be dependent on cluster size. This is indicated from Figure 8, where at p_0 = 15 bar and r_c ~250 Å, the cluster expansion mechanism is relatively rapid, and the collisional heating in the sub-critical density plasma after cluster disassembly, is also less effective due to the considerably lower plasma density. Therefore, the optimum intensity is mainly determined by the ionisation threshold intensity of I_L ~2 × 10^{14} W cm^{-2}. For the larger clusters of ~520–720 Å radius, both mechanisms are important and the optimum incident laser intensity is therefore higher. Due to this, the laser absorption also falls much less rapidly with increasing incident laser intensity. As

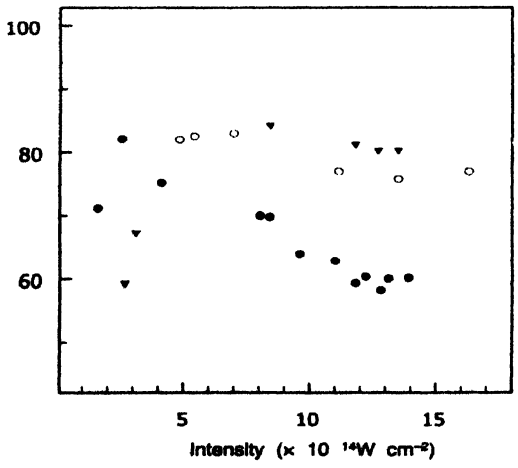

Figure 8. Variation of percentage absorption with incident laser energy for argon gas operated at different (● – 15 bar, O — 40 bar, ▼ – 60 bar) backing pressures.

bulk plasma heating takes place after the clusters have exploded, the X-ray emission signal strength is determined by both the initial cluster size, and the average plasma density in the laser focal region. This is shown in Figure 9, where X-ray signal strength increases steadily with increasing backing pressure.

7. Conclusion

The various characterisation studies carried out using

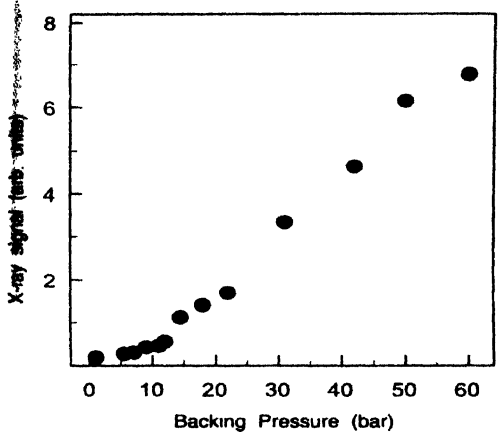

Figure 9. Variation of X-ray signal strength with backing pressure.

different nozzles have shown that hypersonic nozzles are far superior to sonic nozzles, in terms of uniform spatial profile, larger cluster size, and much reduced gas throughput. The control of cluster size through appropriate choice of nozzle parameters and backing pressure, provides an important tool for carrying laser plasma interaction studies. We have explained our observations of highly efficient absorption and the presence of strong X-ray emission from cluster plasmas irradiated by moderately intense multi-picosecond laser light. Our experimental results indicate the possibility of using such targets for single shot, debris-free source, for applications like X-ray contact microscopic imaging of live biological specimens.

Acknowledgments

The authors gratefully acknowledge the help and support provided by C P Navathe and H R Bundel, in the electronics and power supply part. The authors also wish to thank V K Senecha for several helpful suggestions and discussions.

References

[1] W G Hogan *Energy from Inertial Fusion* (Vienna : International Atomic Agency) (1995)

[2] H Fiedorowicz, A Bartnik, Y Li, P Lu and E Fill *Phys. Rev. Lett.* **76** 415 (1996)

[3] A D Stead, R A Cotton, J G Duckett, J A Goode, A M Page and T W Ford *J. X-Ray Sci. Technol.* **5** 52 (1995)

[4] M Chaker, B La Fontaine, C Y Cote, J C Kieffer, H Pepin, M H Talon, G D Enright and D M Villeneuve *J. X-ray Sci. Technol.* **B10** 3239 (1992)

[5] M Wieland, T Wilhelm, M Faubel, Ch Ellert, M. Schmidt and O Sublemontier *Appl. Phys.* **B72** 591 (2001)

[6] I C E Turcu and J B Dance *X-Rays from Laser Plasmas* (Chichester : John Wiley) Ch 7, Sec 7.2 p219 (1999)

[7] T Ditmire, T Donnelly, A M Rubenchik, R W Falcone and M D Perry *Phys. Rev.* **A53** 3379 (1996)

[8] A McPherson, B D Thompson, A B Borisov, K Boyer and C K Rhodes *Nature* **370** 631 (1994)

[9] T Ditmire, R A Smith, J W G Tisch and M H R Hutchinson *Phys. Rev. Lett.* **78** 3121 (1997)

[10] T Shiraishi, M Mori and K Kondo *Phys. Rev.* **A65** 045201 (2002)

[11] M Lezius, S Dobosz, D Normand and M Schmidt *J. Phys.* **B30** L251 (1997)

[12] V P Krainov and M B Smirnov *Phys. Rep.* **370** 237 (2002)

[13] M Suzuki, H Daido, Woo Choi, W Yu, K Nagai, T Norimatsu and H Fiedorowicz *Phys. Plasmas* **10** 227 (2003)

[14] H Fiedorowicz, A Bartnik, M Szczurek, H Daido, N Sakaya, V Kmetik, Y Kato, M Suzuki, M Matsumura, J Tajima, T Nakayama and T Wilhein *Opt. Commun.* **163** 103 (1999)

[15] T Ditmire, J Zweiback, V P Yanovsky, T E Cowan, G Hays and K B Wharton *Nature* **398** 489 (1999)

[16] O F Hagena *Rev. Sci. Instrum.* **63** 2374 (1992)

[17] O F Hagena and W Obert *J. Chem. Phys.* **56** 1793 (1972)

[18] M Born and E Wolf *Principles of Optics* (Oxford : Pergamon) Ch 2, Sec 2.3 p87 (1980)

[19] S Sailaja, R A Khan, P A Naik and P D Gupta *IEEE Trans. Pl. Sci.* (in press) (2005)